HHS Public Access

Author manuscript

Cell Rep. Author manuscript; available in PMC 2015 September 12.

Published in final edited form as:

Cell Rep. 2015 August 4; 12(5): 743–751. doi:10.1016/j.celrep.2015.06.064.

Neurolastin, a dynamin family GTPase, regulates excitatory synapses and spine density

Richa Madan Lomash[1], **Xinglong Gu**[2], **Richard J. Youle**[3], **Wei Lu**[2], and **Katherine W. Roche**[1,*]

[1]Receptor Biology Section, National Institute of Neurological Disorders and Stroke (NINDS), National Institutes of Health (NIH), Bethesda, MD 20892 (USA)

[2]Synapse and Neural Circuit Research Unit, NINDS, NIH, Bethesda, MD 20892 (USA)

[3]Surgical Neurology Branch, NINDS, NIH, Bethesda, MD 20892 (USA)

SUMMARY

Membrane trafficking and spinogenesis contribute significantly to changes in synaptic strength during development and in various paradigms of synaptic plasticity. GTPases of the dynamin family are key players regulating membrane trafficking. Here, we identify a brain-specific dynamin family GTPase, neurolastin (RNF112/Znf179), with closest homology to atlastin. We demonstrate that neurolastin has functional GTPase and RING domains, making it a unique protein identified with this multi-enzymatic domain organization. We also show that neurolastin is a peripheral membrane protein, which localizes to endosomes and affects endosomal membrane dynamics via its RING domain. In addition, neurolastin knockout mice have fewer dendritic spines, and rescue of the wildtype phenotype requires both the GTPase and RING domains. Furthermore, we find fewer functional synapses and reduced paired pulse facilitation in neurolastin knockout mice. Thus, we identify neurolastin as a dynamin family GTPase that affects endosome size and spine density.

INTRODUCTION

Members of the dynamin family of GTPases play central roles in regulating vesicular trafficking and membrane transport. The basic architecture of the dynamin family of proteins includes the GTPase catalytic domain, the middle domain, and a GTPase effector domain (GED). Homo-oligomerization is an important part of the catalytic process as these

*Correspondence should be addressed to: Dr. Katherine W. Roche (rochek@ninds.nih.gov), Receptor Biology Section, NINDS, Porter Neuroscience Research Center, Building 35, Room 2C-903, Bethesda, MD 20892-3704.

AUTHOR CONTRIBUTIONS

R.M.L. designed experiments, and performed all biochemical and imaging experiments. R.M.L. and K.W.R. wrote the manuscript. W.L. and X.G. designed and conducted electrophysiology experiments. K.W.R. and R.J.Y. helped design experiments and supervised the project.

The authors declare no conflict of interest.

GTPases undergo assembly-stimulated GTP hydrolysis (Gasper et al., 2009) and is mediated by the middle domain, along with the GED. For purposes of membrane remodeling, these proteins are either embedded or peripherally associated with membranes via specific domains or motifs. Different members associate with specific membranes and catalyze membrane remodeling in a GTPase-dependent manner (Heymann and Hinshaw, 2009). For instance, dynamin associates with the plasma membrane, atlastin with ER membrane, and mitofusin is present on the mitochondrial membrane (Ferguson and De Camilli, 2012). Both atlastin and mitofusin play a major role in maintenance of normal ER and mitochondrial morphology, respectively (Hu et al., 2009; Zhang and Chan, 2007). Various isoforms of dynamin have been implicated in regulating synaptic vesicle (SV) trafficking at the plasma membrane (Raimondi et al., 2011).

Another important mechanism regulating vesicular trafficking is ubiquitination, a post-translational modification. Key players involved in ubiquitination include E3 ubiquitin ligases, which catalyze the transfer of ubiquitin from the cognate ubiquitin-conjugating enzyme (E2) to the substrate (Deshaies and Joazeiro, 2009). E3 ligases containing a RING domain are known to play diverse roles in endosomal sorting and synaptic plasticity (Haglund and Dikic, 2012; Mabb and Ehlers, 2010). For example, RNF167 regulates synaptic transmission by ubiquitinating AMPARs and targeting them to the lysosomes (Lussier et al., 2012) and *Drosophila* E3 ligases regulate endosomal trafficking via ubiquitination of VAMP3 (Yamazaki et al., 2013).

Of the many identified RING E3 ligases, one is RNF112 (Znf179/Zfp179/Bfp), which we have named neurolastin based on our results. It maps within the chromosomal region encoding the Smith-magenis syndrome (Kimura et al., 1997), a developmental disorder and has known homologs only in higher eukaryotes. Though neurolastin has been shown to be brain-specific with a temporal increase in its expression (Orimo et al., 1998; Pao et al., 2011), there is no direct evidence demonstrating its E3 ligase activity and a very limited understanding about the overall function of this protein. Only recently, a few studies have suggested that neurolastin is important for neuronal differentiation and neurogenesis (Lin et al., 2013; Pao et al., 2011).

In this study, we characterize neurolastin as a dynamin family GTPase, which contains multi-enzymatic domains. Because it shows closest homology to atlastin and is specifically expressed in the nervous system, we name it neurolastin. Neurolastin exhibits GTPase and E3 ligase activities, is peripherally attached to membranes, and localizes to multiple endocytic vesicles. To delineate the importance of neurolastin, we generated neurolastin knockout mice (KO), which have smaller endosomes, less synapses, reduced dendritic spine density and reduced paired pulse facilitation. While endosomal localization and a functional RING domain of neurolastin affect the endosome size, both RING and GTPase domains are essential to maintain spine density. The characterization of neurolastin expands the dynamin family and adds to our current knowledge of the different roles played by dynamin family GTPases in neuronal physiology.

RESULTS

Neurolastin is a functional GTPase, related to the dynamin family of proteins

To understand the function of neurolastin, we first searched for conserved domains within the protein using the NCBI database, and found an apparent GTPase domain, a RING domain, and two potential transmembrane domains. Further bioinformatic analyses suggested that the GTPase domain of neurolastin shows homology with dynamin family members (Figure 1A). Sequence alignment revealed that neurolastin contains the key residues essential for nucleotide binding and hydrolysis in the canonical motifs (G1, G2, G3 and G4) of the GTPase domain. Additionally, it also suggests that the G4 motif of neurolastin is most closely related to guanylate-binding proteins (GBPs) and atlastin (Figure 1B).

To test the predicted activity experimentally, we purified neurolastin with an N-terminal GST-tag and used it in an *in vitro* GTP hydrolysis assay. We found that neurolastin does indeed hydrolyze GTP. Interestingly, it has the ability to hydrolyze GTP to its monophosphate form, GMP (Figure 1C). To delineate the function of the GTPase domain, we generated a GTPase activity-defective mutant. Different GTPase mutants in the G4 motif of GBPs and atlastin have been characterized previously (Byrnes and Sondermann, 2011; Praefcke et al., 2004). Based on these reports, we substituted Arg (R) with Glu (Q) in the G4 motif to generate the GTPase mutant (R340Q) of neurolastin. Neurolastin R340Q displays a nearly 50% reduction both in GDP and GMP production, when compared to WT (Figure 1D and 1E).

The ability to hydrolyze GTP and oligomerize are characteristic of dynamin family GTPases; these being mediated by the GTPase domain in conjunction with the GED and middle domains. Although the middle domains of dynamin family members lack sequence conservation or detectable similarity to known structural motifs, they contain a predicted coiled-coil region (Heymann and Hinshaw, 2009). In accordance with this, we searched for coiled-coil regions in neurolastin and found that the analogous region (residues 472–565) shows a high probability of coiled-coils (Figure S1A), which potentially form the middle domain. Using immunoprecipitation, we checked if neurolastin could self-associate. We co-expressed HA- and Flag-neurolastin in HEK cells, specifically isolated HA-neurolastin using an HA antibody and detected Flag-neurolastin, demonstrating that neurolastin could self-associate (Figure 1F).

Neurolastin is a functional E3 ligase

In addition to the GTPase domain, neurolastin also has an E3 ubiquitin ligase domain. Sequence analysis shows that neurolastin has a C3HC4 type RING domain and key residues important for zinc coordination are conserved (Figure 2A). We next tested the E3 ligase activity of neurolastin in an *in vitro* ubiquitination assay. We incubated GST-neurolastin and Myc-ubiquitin in an ATP regenerating system with HeLa cell lysate that serves as a source of potential substrates. We observed the formation of poly-ubiquitin conjugates when neurolastin was added exogenously to the reaction (Figure 2B), confirming that neurolastin is a functional E3 ligase. All E3 ligases have cognate E2s. To identify the specific E2 for

neurolastin, we performed a substrate independent assay using purified E1, GST-neurolastin, and Myc-ubiquitin and tested for the ability of neurolastin to auto-ubiquitinate in the presence of different E2s. Of the multiple E2s tested, ubiquitination by GST-neurolastin was observed in the presence of three E2s, namely UBE2D1, UBE2D2, and UBE2D3 (Figure 2C). We also used a dominant negative mutant (C85A) of the identified E2s and observe no ubiquitination, demonstrating the specificity of the E2s identified.

Neurolastin is peripherally associated with membranes via its C-terminus and localizes to endocytic vesicles

Neurolastin, like atlastin, has hydrophobic regions predicted to be transmembrane domains (570–625) based on different algorithms (Figure S1B). To determine whether neurolastin is an integral membrane protein, we expressed HA-tagged neurolastin in HEK cells, separated the membrane and cytosolic fraction by high-speed centrifugation, and examined the presence of neurolastin by immunoblotting. Surprisingly, we found that unlike atlastin, neurolastin is present both in the membrane and cytosolic fractions (Figures 2D) suggesting that the analogous hydrophobic regions of neurolastin are not membrane spanning domains. Although neurolastin is present in the cytosolic fraction, it is also associated with membranes. To characterize the interaction of neurolastin with membranes, we lysed membranes in Tx-114 and separated the integral and peripheral membrane proteins. Neurolastin separates in the aqueous phase, whereas atlastin is found in the detergent phase (Figure 2E), consistent with neurolastin being peripherally associated with the membrane. In contrast, atlastin is a bonafide integral membrane protein. We determined the region important for membrane association by examining the presence of neurolastin full-length (1–654), N-terminal deletion (158–654) and C-terminal deletion (1–563) in the membrane and cytosolic fractions. We find a negligible amount of neurolastin containing the C-terminal deletion in the membrane fraction compared to the N-terminal deletion, which is present in quantities similar to full-length neurolastin (Figure 2F). Interestingly, the region deleted from the C-terminus has a stretch of hydrophobic residues (Figure S1C). These results indicate that neurolastin is peripherally associated with membranes via its C-terminal region.

To determine the localization of neurolastin, HA-tagged neurolastin was expressed in HeLa cells and examined. Neurolastin showed a diffuse and punctate localization, representing the cytosolic and membrane fractions of neurolastin. Neurolastin does not colocalize with distinct organelles (Figure 2G). However, immunofluorescence microscopy revealed that neurolastin is localized to endosomes, as it shows partial colocalization with different endosomal markers (Figure 2H).

Generation and characterization of neurolastin KO mice

To study the functional significance of neurolastin *in vivo*, we generated a KO reporter mouse strain (Figure S2A). The KO was confirmed by genotyping PCR (Figure S2B) and immunoblotting using a neurolastin antibody. The specificity of the antibody was tested by Western blot analysis of HEK cells expressing neurolastin (Figure S2C). Though the antibody picks up multiple bands, it specifically recognizes endogenous neurolastin from brain lysate of WT mice, whereas no corresponding signal was seen in the KO mice (Figure

S2D). The KO mice are viable and show no obvious defects, although we observe some breeding inconsistency (data not shown). Adult animals (one year old) were subjected to a detailed phenotypic examination. Interestingly, the only difference observed was a reduction in the size of brains (~10%) of the KO animals, whereas other organs were similar to WT (Figure S2E).

Neurolastin affects endosomal membrane dynamics via its RING domain

Because neurolastin shows endosomal localization, we examined if it plays any role in modulating endosomal membrane dynamics. In neurons, we co-expressed neurolastin (WT or mutants) with YFP-EEA1 (to label endosomes) and examined endosomal volume. Interestingly, we observe that neurolastin H97W (RING mutant), leads to a significant reduction in large endosomes (volume greater than 0.1 μm^3) and an increase in small endosomes, whereas no change in endosome size is observed upon expression of neurolastin WT or neurolastin R340Q (Figure 3A and 3B). Based on this observation, we compared the size of endosomes in WT and KO neurons by light microscopy and found a significant reduction in larger endosomes in KO mice (Figure 3C and 3D). Next, we tried to rescue the endosomal defect by expressing neurolastin (WT or mutants) in KO neurons. We find that the endosomal phenotype can be rescued by expressing neurolastin WT or neurolastin R340Q (GTPase mutant) and not by neurolastin H97W, the RING mutant (Figure 3E and 3F). We examined if there was any change in the localization of neurolastin mutants with endosomal markers in HeLa cells. Interestingly, we observe a clear mislocalization of neurolastin H97W (RING mutant) onto mitochondria (Figure S3). These results show that a functional RING domain is essential for endosomal localization of neurolastin, which in turn is important for maintaining endosomal size.

Neurolastin is important for excitatory neurotransmission

Because neurolastin is localized to vesicles and impacts endosome size, we hypothesized it might affect dendritic spines. Hence, we analyzed the effect of neurolastin expression on dendritic spine density. Neurolastin (WT or mutants) and GFP were co-expressed in neurons and the number of dendritic spines counted. Interestingly, we observed that expression of neurolastin WT led to a significant increase in spine density, whereas expression of either neurolastin R340Q (GTPase mutant) or neurolastin H97W (RING mutant) had no effect on spine density (Figures 4A and 4B). These results indicate a requirement of functional GTPase and RING domains of neurolastin for increasing spine density. Importantly, we find fewer dendritic spines in KO mice *in vivo* (Figures 4C and 4D). Finally, we tested if exogenous neurolastin could rescue the spine density defect in KO mice. Neurons cultured from KO mice were transfected with neurolastin (WT or mutants) and the number of spines counted. We find that only WT neurolastin could rescue the spine density deficit whereas the RING and GTPase mutants could not (Figures 4E and 4F).

Finally, we investigated if neurolastin regulates excitatory neurotransmission. We recorded mEPSCs (miniature excitatory postsynaptic currents) in CA1 pyramidal neurons of acute hippocampal slices from mice (P14–18). A significant decrease in the frequency of mEPSCs in KO mice was observed, although the amplitude and mini decay remained unchanged (Figures 5A–5D), suggesting a reduced number of functional synapses, whereas the synaptic

strength remains unaltered. Moreover, we observed a change in the levels of glutamate receptors in KO mice compared to WT (Figures 5E and 5F), most notably finding that the AMPAR subunits, GluA1 and GluA2, are significantly reduced in the synaptic fraction. Furthermore, the levels of NMDAR subunits are differentially regulated, with a reduction in GluN2A compared to an increase in GluN2B in KO mice. These changes are most consistent with a delay in synaptic maturation. We also measured EPSCs from hippocampal slices and compared the paired pulse facilitation between WT and KO mice. We observed reduced paired pulse facilitation in KO mice (Figure 5G and 5H) confirming a presynaptic contribution of neurolastin. We also observed that neurolastin is present in multiple subcellular fractions including enriched SVs and post-synaptic density (PSD) (Figure S4), showing biochemical evidence for a pre- and post-synaptic role. Together, these results show that the absence of neurolastin leads to a compromise in synaptic transmission.

DISCUSSION

Dynamin and its isoforms have been studied for decades and are central players in regulating SV endocytosis (Ferguson and De Camilli, 2012). Other members of the dynamin family play diverse roles in fission and fusion of organelles (Heymann and Hinshaw, 2009). The last mammalian member added to this family was atlastin over a decade ago (Zhao et al., 2001). Since that time it has been shown that atlastin plays an important role in driving the homotypic fusion of ER membranes (Hu et al., 2009).

We have now identified a brain-specific GTPase of this family, neurolastin. Based on its sequence, neurolastin is most closely related to atlastin; but, surprisingly, it is not a transmembrane protein like atlastin. We show it is a peripheral membrane protein, making neurolastin similar, in this regard, to the founding member, dynamin. However, neurolastin can hydrolyze GTP to GMP, clearly distinguishing it from dynamin. This feature aligns it more closely to GBPs and atlastins, the only two classes of proteins that catalyze GTP hydrolysis to GMP (Byrnes and Sondermann, 2011; Schwemmle and Staeheli, 1994). The presence of a RING domain and it being a functional E3 ligase makes neurolastin a unique GTPase. Though proteins with multi-functional domains have been previously reported, none of the dynamin family GTPase possesses functional multi-enzymatic domains.

We also find that neurolastin localizes to endocytic vesicles. Importantly, it does not localize to the ER, mitochondria or plasma membrane, membranes already targeted by known dynamin family members (Ferguson and De Camilli, 2012). Vesicle budding and subsequent membrane fission occurs throughout the secretory and endocytic pathway. Although dynamin drives the scission of endocytic vesicles at the plasma membrane, it does not affect most events in the endocytic pathway (Ferguson and De Camilli, 2012). Thus, localization of neurolastin to different endocytic vesicles implicates a substantial role in endocytic membrane dynamics. Furthermore, changes in the expression of different endocytic proteins upon shRNA-mediated knockdown of neurolastin have been reported (Pao et al., 2011). Additionally, we find that neurolastin KO mice have smaller endosomes. Our results suggest that localization of neurolastin to endosomes involving its RING domain is important for maintaining endosome size. Along similar lines, it has been reported that the *Drosophila*

Goliath and Godzilla E3 ligases, and one of their human homologs, RNF167, located on endosomes regulate the endosome size via ubiquitination (Yamazaki et al., 2013).

Many proteins, including GTPases and E3 ligases, regulate dendritic spines by different mechanisms including spine morphogenesis, and changes in dendritic spines have been associated with various neurological disorders. For example, TRIM3, a RING finger protein degrades its substrate, GKAP, decreasing it at the postsynaptic sites resulting in smaller dendritic spines (Hung et al., 2010). Although, proteins from the Rho family of GTPases play a major role in altering spine morphology via cytoskeletal rearrangements (Lin and Koleske, 2010), it has also been reported that a dynamin-3 splice variant is important for maintaining dendritic spine morphology (Gray et al., 2005). More recently, atlastin's GTPase activity has been implicated in dendritic morphogenesis (Gao et al., 2013). Interestingly, we observe significantly lesser dendritic spines in neurolastin KO mice. Furthermore, spine density is dependent on the presence of functional GTPase and RING domains of neurolastin.

Numerous studies in the literature show that endosomes play a major role in regulating long-term potentiation (LTP) and long-term depression (LTD), two of the most well studied forms of synaptic plasticity, by controlling the number of AMPARs at the synapse. AMPARs are sorted in endosomal compartments and either recycled to the PM (LTP) or targeted to lysosomes for degradation (LTD) (Huganir and Nicoll, 2013). In neurolastin KO mice, we observe smaller endosomes and a decrease in synaptic AMPARs, implicating the limited ability of neurons to efficiently traffic AMPARs to the synapse. Furthermore, we observe a dramatic decrease in dendritic spines in the neurolastin KO mice, a phenotype that is tightly linked to AMPAR trafficking and exocytosis. Indeed, previous reports show that recycling endosomes modulate spine growth by exocytosis during synaptic plasticity (Park et al., 2006). Thus, these observations in the neurolastin KO suggest a trafficking defect due to altered endosomal membrane dynamics. While the smaller PPF ratio in the KO suggests higher neurotransmitter release probability of the presynaptic neurons, the reduced spine density may underlie the observed deficits in mEPSC frequency in the neurolastin KO.

Our observations in neurolastin KO mice of a strong deficit in mEPSC frequency, compromised paired pulse facilitation and reduced dendritic spine density suggest its significant role at both the pre- and post-synapse. This behavior is similar to dynamin, which although mostly characterized as presynaptic has been shown to localize at the post synapse and affect AMPAR trafficking (Carroll et al., 1999; Jaskolski et al., 2009; Lu et al., 2007). Interestingly, the GTPase activity of dynamin, which is important for SV endocytosis, is not responsible for these effects. Instead, they are mediated by interaction of dynamin with the post-synaptic protein Homer, through its proline-rich domain. Thus, studies highlight the pleiotropic effects of dynamin being driven by its different domains. In a similar fashion, results presented in this study also suggest pleiotropic effects of neurolastin on endosome size, spine density and a presynaptic function, involving different domains present on neurolastin. These results are supported by our findings that neurolastin is present in the microsomal, PSD and SV fractions. The observed phenotypes in KO mice open a wide range of questions as to which domain and what mechanism is underlying these effects. Additionally, different reports of other GTPases reveal interplay between the GTPase

activity and ubiquitin-dependent degradation affecting the mitochondrial membrane fusion (Cohen et al., 2011; Karbowski et al., 2007). However, in all cases, there is involvement of two separate proteins harboring the RING and GTPase domains. Interestingly, in neurolastin both the domains reside together, suggesting a potential interplay.

In conclusion, we identify a member of the dynamin family GTPases that contains a RING domain and plays a crucial role in synaptic transmission. Even though the neurolastin KO mice are viable, the notable change in spine density and endosome size suggests its potential role in pathogenesis of different neurological disorders. Investigating the molecular mechanisms underlying the observed phenotypes will enhance our understanding of membrane trafficking, dendritic spines dynamics, and different mechanisms that govern synaptic plasticity.

EXPERIMENTAL PROCEDURES

Neuronal cultures, antibodies and reagents

DNA constructs, reagents and antibodies are detailed in Supplemental Experimental Procedures. Primary neurons were cultured from embryonic day 18 Sprague-Dawley rats as described previously (Roche and Huganir, 1995).

Biochemical characterization

GTPase activity assay—Different concentrations of GST-tagged neurolastin (71–563) were incubated with 100 nM α-^{32}P-GTP in the presence of 2 mM $MgCl_2$ for 60 min at 37°C. The reaction was stopped by adding 2 mM EDTA and the products were resolved by thin layer chromatography using 0.6 M NaH_2PO_4 pH 3.5 as the solvent. For comparison of GDP and GMP production between neurolastin WT and neurolastin R340Q, protein was used at a concentration of 0.5 μM. Percent hydrolysis was estimated by calculating the intensity of the corresponding spots obtained using ImageJ.

E3 ligase activity assay: 1 μM GST-neurolastin (71–563) was incubated with HeLa S-100 fraction (60 μg), DTT (100 nM), ubiquitin aldehyde (1 μg) and Myc-ubiquitin (10 μg) in an ATP-regenerating buffer system for 60 min at 30°C. The products were resolved on a gradient gel and immunoblotted with α-FK1 antibody. For the *in vitro* substrate-independent E3 ligase activity assay, purified GST-neurolastin, E1 (100 ng), E2 (200 ng) and Myc-ubiquitin (10 μg) were incubated in an ATP regenerating buffer system for 60 min at 30°C. The products were resolved on a gradient gel and immunoblotted with α-Myc antibody. Membrane association and subcellular fractionation were performed using standard procedures and are described in Supplemental Experimental Procedures.

Electrophysiology and Immunofluorescence

Electrophysiology was performed on hippocampal slices prepared from P14–18 animals and is detailed in Supplemental Experimental Procedures. Immunofluorescence microscopy was performed using standard methods.

Determining the volume of endosomes: DIV10 rat hippocampal neurons were co-transfected with YFP-EEA1 and neurolastin-HA (WT, R340Q or H97W) cloned into the pCAG vector using Lipofectamine 2000. The cells were fixed at DIV13 and stained with α-HA antibody to detect neurolastin. For rescue experiments, P0-P1 hippocampal neurons from neurolastin KO mice were used and the experiment was performed as described above. For comparing the endosomal volume between WT and KO, mouse hippocampal neurons were cultured at P0-P1 and stained at DIV13 for endogenous EEA1. Subsequently, Z-stacks were captured using a 63X oil immersion objective of a LSM 510 Meta Zeiss confocal microscope. The volume of endosomes was calculated from Z-stacks using Volocity analysis software. The threshold was kept constant for all images in each experiment. Objects smaller than 0.01 μm^3 were disregarded. Subsequently the volume of all objects in selected regions (three dendritic regions per neuron) was measured. 10–15 neurons were analyzed in each experiment per given condition. Endosomes with different volumes were binned into two groups (with a volume either less or more than 0.1 μm^3). The percentage of endosomes per neuron in both the groups was calculated and data is presented as mean ± SEM.

Dendritic spine density: DIV14 rat hippocampal neurons were co-transfected with GFP (to fill spines) and neurolastin-HA (WT, R340Q or H97W) using Lipofectamine 2000. The cells were fixed at DIV18 and stained with α-HA antibody to detect neurolastin. Subsequently, Z-stacks were captured using a 63X oil immersion objective of LSM 510 Meta Zeiss confocal microscope. Spines per 10 um were counted from three secondary/tertiary dendrites per neuron using Metomorph analysis software. 10–15 neurons were analyzed in each condition per experiment. For rescue experiments, hippocampal neurons were cultured from P0-P1 neurolastin KO mice and the experiment was performed as described above. A projection image was created using different optical sections (0.35 μm) and is presented. The average number of spines per neuron was calculated and data is presented as mean ± SEM.

Statistical analysis

An unpaired two-tailed t-test was used to determine the significance of the data from independent experiments, as indicated.

Supplementary Material

Refer to Web version on PubMed Central for supplementary material.

ACKNOWLEDGEMENTS

We thank Stephanie McNeil who initiated this study as part of her doctoral thesis at Johns Hopkins University. We also thank John D. Badger II and Kai Chang for technical assistance. We are grateful to Dr. James Pickel and the NIMH transgenic facility for their help in generation of the KO mouse. We thank the NINDS sequencing, imaging and animal facility for their assistance. We would like to thank members of the Roche, Blackstone and Youle laboratory for helpful discussions. This research was supported by the NINDS Intramural Research Program (R.M.L., X.G., W.L., R.J.Y. and K.W.R.).

REFERENCES

Byrnes LJ, Sondermann H. Structural basis for the nucleotide-dependent dimerization of the large G protein atlastin-1/SPG3A. Proceedings of the National Academy of Sciences of the United States of America. 2011; 108:2216–2221. [PubMed: 21220294]

Carroll RC, Beattie EC, Xia H, Luscher C, Altschuler Y, Nicoll RA, Malenka RC, von Zastrow M. Dynamin-dependent endocytosis of ionotropic glutamate receptors. Proceedings of the National Academy of Sciences of the United States of America. 1999; 96:14112–14117. [PubMed: 10570207]

Cohen MM, Amiott EA, Day AR, Leboucher GP, Pryce EN, Glickman MH, McCaffery JM, Shaw JM, Weissman AM. Sequential requirements for the GTPase domain of the mitofusin Fzo1 and the ubiquitin ligase SCFMdm30 in mitochondrial outer membrane fusion. Journal of cell science. 2011; 124:1403–1410. [PubMed: 21502136]

Deshaies RJ, Joazeiro CA. RING domain E3 ubiquitin ligases. Annual review of biochemistry. 2009; 78:399–434.

Ferguson SM, De Camilli P. Dynamin, a membrane-remodelling GTPase. Nature reviews Molecular cell biology. 2012; 13:75–88. [PubMed: 22233676]

Gao Y, Jiang T, Qu C, Tao H, Cao H, Zhao Y, Wang Y, Qu J, Chen JG. Atlastin-1 regulates dendritic morphogenesis in mouse cerebral cortex. Neuroscience research. 2013; 77:137–142. [PubMed: 23999326]

Gasper R, Meyer S, Gotthardt K, Sirajuddin M, Wittinghofer A. It takes two to tango: regulation of G proteins by dimerization. Nature reviews Molecular cell biology. 2009; 10:423–429. [PubMed: 19424291]

Gray NW, Kruchten AE, Chen J, McNiven MA. A dynamin-3 spliced variant modulates the actin/cortactin-dependent morphogenesis of dendritic spines. Journal of cell science. 2005; 118:1279–1290. [PubMed: 15741233]

Haglund K, Dikic I. The role of ubiquitylation in receptor endocytosis and endosomal sorting. Journal of cell science. 2012; 125:265–275. [PubMed: 22357968]

Heymann JA, Hinshaw JE. Dynamins at a glance. Journal of cell science. 2009; 122:3427–3431. [PubMed: 19759282]

Hu J, Shibata Y, Zhu PP, Voss C, Rismanchi N, Prinz WA, Rapoport TA, Blackstone C. A class of dynamin-like GTPases involved in the generation of the tubular ER network. Cell. 2009; 138:549–561. [PubMed: 19665976]

Huganir RL, Nicoll RA. AMPARs and synaptic plasticity: the last 25 years. Neuron. 2013; 80:704–717. [PubMed: 24183021]

Hung AY, Sung CC, Brito IL, Sheng M. Degradation of postsynaptic scaffold GKAP and regulation of dendritic spine morphology by the TRIM3 ubiquitin ligase in rat hippocampal neurons. PloS one. 2010; 5:e9842. [PubMed: 20352094]

Jaskolski F, Mayo-Martin B, Jane D, Henley JM. Dynamin-dependent membrane drift recruits AMPA receptors to dendritic spines. The Journal of biological chemistry. 2009; 284:12491–12503. [PubMed: 19269965]

Karbowski M, Neutzner A, Youle RJ. The mitochondrial E3 ubiquitin ligase MARCH5 is required for Drp1 dependent mitochondrial division. The Journal of cell biology. 2007; 178:71–84. [PubMed: 17606867]

Kimura T, Arakawa Y, Inoue S, Fukushima Y, Kondo I, Koyama K, Hosoi T, Orimo A, Muramatsu M, Nakamura Y, et al. The brain finger protein gene (ZNF179), a member of the RING finger family, maps within the Smith-Magenis syndrome region at 17p11.2. American journal of medical genetics. 1997; 69:320–324. [PubMed: 9096764]

Lin DY, Huang CC, Hsieh YT, Lin HC, Pao PC, Tsou JH, Lai CY, Hung LY, Wang JM, Chang WC, et al. Analysis of the interaction between Zinc finger protein 179 (Znf179) and promyelocytic leukemia zinc finger (Plzf). Journal of biomedical science. 2013; 20:98. [PubMed: 24359566]

Lin YC, Koleske AJ. Mechanisms of synapse and dendrite maintenance and their disruption in psychiatric and neurodegenerative disorders. Annual review of neuroscience. 2010; 33:349–378.

Lu J, Helton TD, Blanpied TA, Racz B, Newpher TM, Weinberg RJ, Ehlers MD. Postsynaptic positioning of endocytic zones and AMPA receptor cycling by physical coupling of dynamin-3 to Homer. Neuron. 2007; 55:874–889. [PubMed: 17880892]

Lussier MP, Herring BE, Nasu-Nishimura Y, Neutzner A, Karbowski M, Youle RJ, Nicoll RA, Roche KW. Ubiquitin ligase RNF167 regulates AMPA receptor-mediated synaptic transmission. Proceedings of the National Academy of Sciences of the United States of America. 2012; 109:19426–19431. [PubMed: 23129617]

Mabb AM, Ehlers MD. Ubiquitination in postsynaptic function and plasticity. Annual review of cell and developmental biology. 2010; 26:179–210.

Orimo A, Inoue S, Ikeda K, Sato M, Kato A, Tominaga N, Suzuki M, Noda T, Watanabe M, Muramatsu M. Molecular cloning, localization, and developmental expression of mouse brain finger protein (Bfp)/ZNF179: distribution of bfp mRNA partially coincides with the affected areas of Smith-Magenis syndrome. Genomics. 1998; 54:59–69. [PubMed: 9806830]

Pao PC, Huang NK, Liu YW, Yeh SH, Lin ST, Hsieh CP, Huang AM, Huang HS, Tseng JT, Chang WC, et al. A novel RING finger protein, Znf179, modulates cell cycle exit and neuronal differentiation of P19 embryonal carcinoma cells. Cell death and differentiation. 2011; 18:1791–1804. [PubMed: 21566658]

Park M, Salgado JM, Ostroff L, Helton TD, Robinson CG, Harris KM, Ehlers MD. Plasticity-induced growth of dendritic spines by exocytic trafficking from recycling endosomes. Neuron. 2006; 52:817–830. [PubMed: 17145503]

Praefcke GJ, Kloep S, Benscheid U, Lilie H, Prakash B, Herrmann C. Identification of residues in the human guanylate-binding protein 1 critical for nucleotide binding and cooperative GTP hydrolysis. Journal of molecular biology. 2004; 344:257–269. [PubMed: 15504415]

Raimondi A, Ferguson SM, Lou X, Armbruster M, Paradise S, Giovedi S, Messa M, Kono N, Takasaki J, Cappello V, et al. Overlapping role of dynamin isoforms in synaptic vesicle endocytosis. Neuron. 2011; 70:1100–1114. [PubMed: 21689597]

Roche KW, Huganir RL. Synaptic expression of the high-affinity kainate receptor subunit KA2 in hippocampal cultures. Neuroscience. 1995; 69:383–393. [PubMed: 8552236]

Schwemmle M, Staeheli P. The interferon-induced 67-kDa guanylate-binding protein (hGBP1) is a GTPase that converts GTP to GMP. The Journal of biological chemistry. 1994; 269:11299–11305. [PubMed: 7512561]

Yamazaki Y, Schonherr C, Varshney GK, Dogru M, Hallberg B, Palmer RH. Goliath family E3 ligases regulate the recycling endosome pathway via VAMP3 ubiquitylation. The EMBO journal. 2013; 32:524–537. [PubMed: 23353890]

Zhang Y, Chan DC. New insights into mitochondrial fusion. FEBS letters. 2007; 581:2168–2173. [PubMed: 17331506]

Zhao X, Alvarado D, Rainier S, Lemons R, Hedera P, Weber CH, Tukel T, Apak M, Heiman-Patterson T, Ming L, et al. Mutations in a newly identified GTPase gene cause autosomal dominant hereditary spastic paraplegia. Nature genetics. 2001; 29:326–331. [PubMed: 11685207]

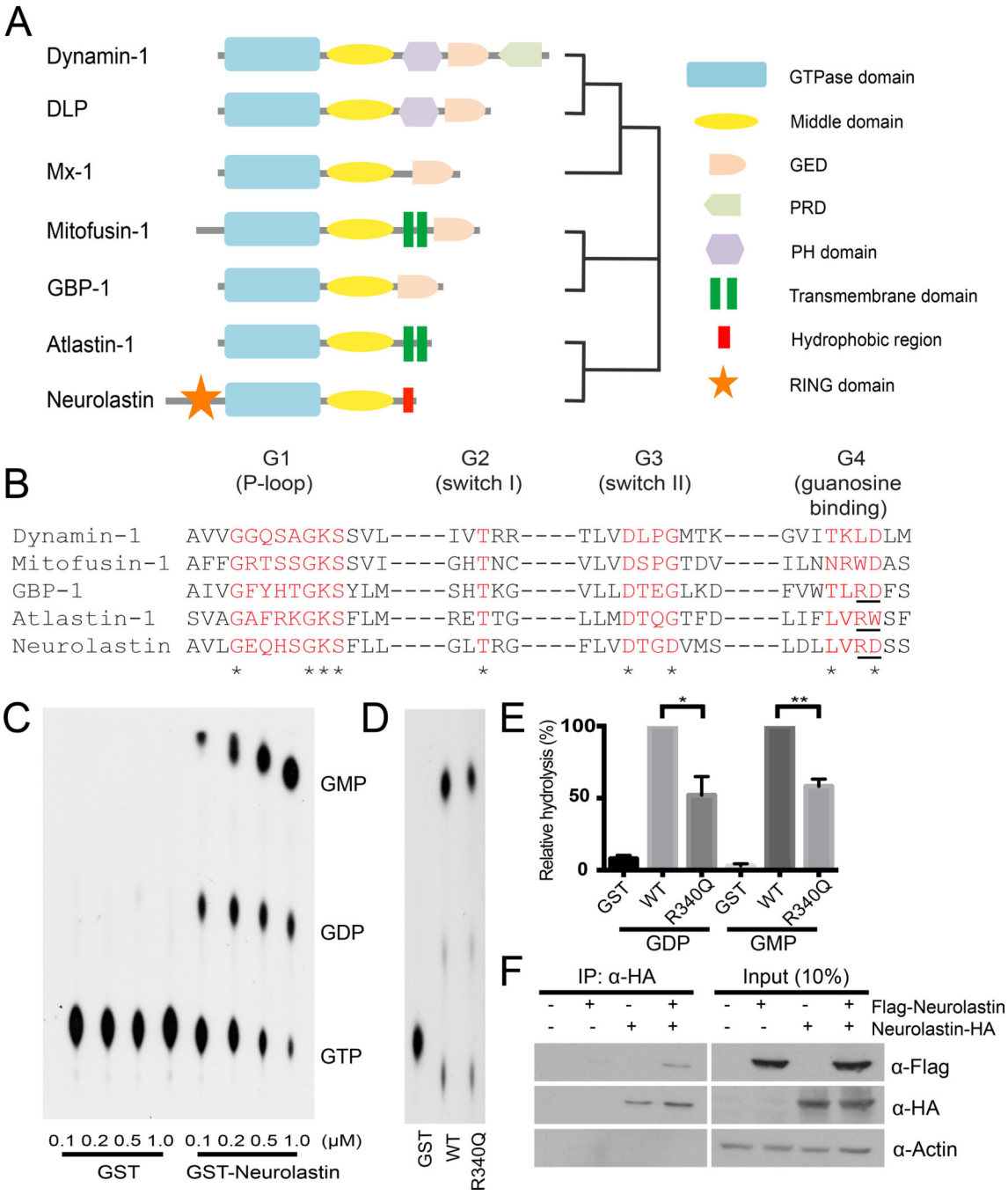

Figure 1. Neurolastin is a functional GTPase, related to the dynamin family of proteins

(A) Schematic of dynamin superfamily proteins showing different domains. Dendrogram based on ClustalW sequence alignment of indicated mouse proteins. Complete sequence of neurolastin is included in Figure S1E.

(B) Sequence alignment of the GTPase domain G1 to G4 motifs (red). Key residues are marked with an asterisk. Underlined residues are signature of GBPs and atlastins and coordinate guanosine binding.

(C) *In vitro* GTPase assay in which purified GST-neurolastin (indicated concentrations) was incubated with α-^{32}P-GTP and the hydrolysis products were separated using Thin-layer chromatography. Autoradiogram shows GDP and GMP as the hydrolysis products of GTP. GST was used as a control.

(D) Characterization of a GTPase mutant. Autoradiogram comparing GTP hydrolysis between WT and R340Q. Graph in **(E)** represents mean ± SEM of relative amount of GDP and GMP produced using 0.5 uM protein (N=3; * $p < 0.01$; ** $p < 0.005$).

(F) Flag-neurolastin and neurolastin-HA were co-expressed, followed by immunoprecipitation with α-HA and immunoblotting with α-Flag antibody (left panel) to determine self-association of neurolastin. Right panel shows the expression of proteins in the cell lysate (input) used for immunoprecipitation.

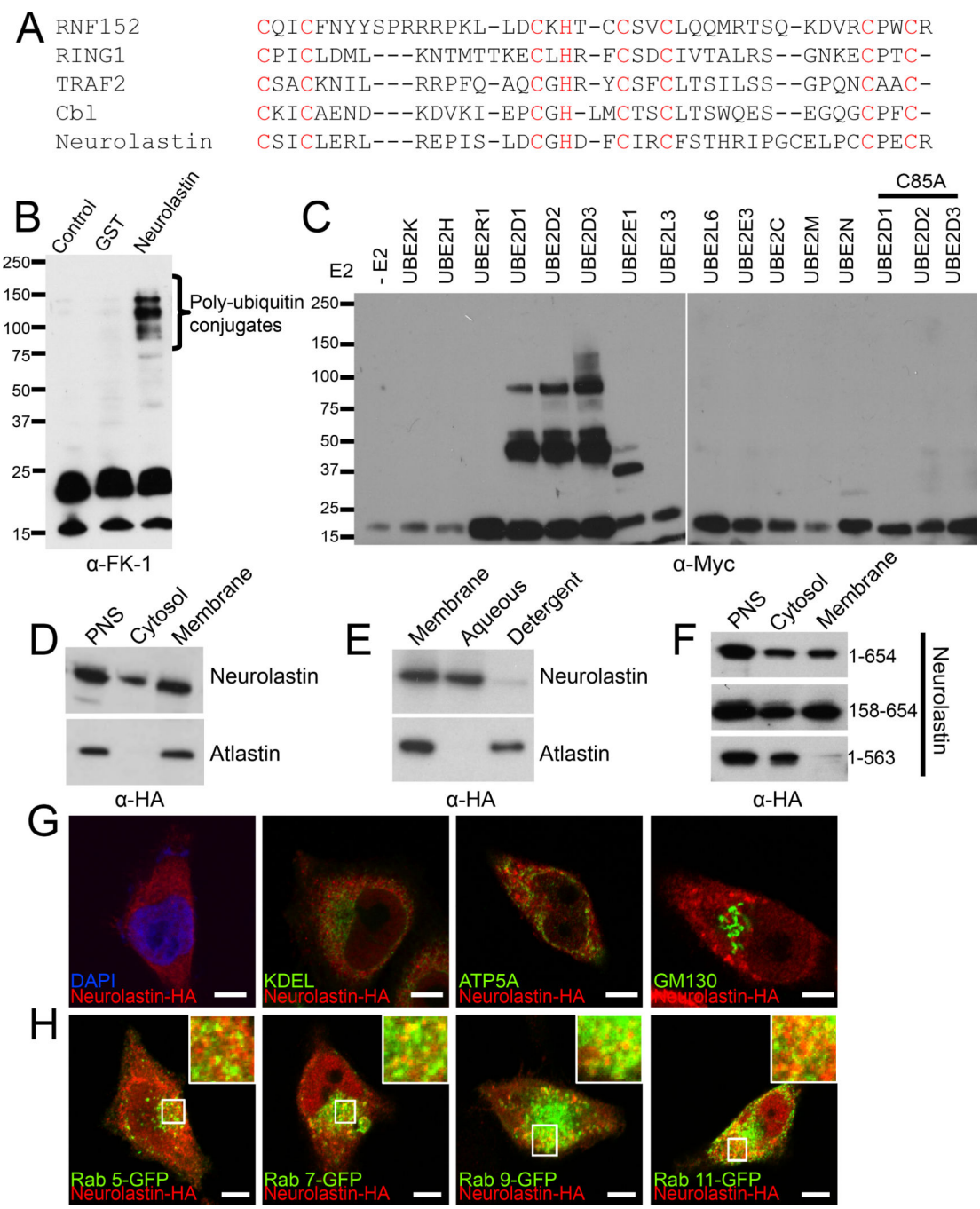

Figure 2. Neurolastin is a functional E3 ligase peripherally associated with membranes

(A) Sequence alignment of the RING (C3HC4) domain of neurolastin with closely related E3 ligases. Conserved residues are highlighted in red.

(B) *In vitro* E3 ligase activity assay in which GST-neurolastin was incubated with HeLa S-100 fraction and Myc-ubiquitin in an ATP-regenerating system. The presence of ubiquitin chains was determined by immunoblotting with α-FK1 antibody, which recognizes poly-ubiquitin conjugates. The control reaction included all components except neurolastin.

(C) Substrate-independent *in vitro* E3 ligase activity assay in which GST-neurolastin was incubated with purified E1 (Uba1), different E2s and Myc-ubiquitin in an ATP-regenerating system. Reaction without E2 and dominant negative form of indicated E2s (C85A) were used as controls. The presence of ubiquitin conjugates was determined by immunoblotting with α-Myc antibody. Signal obtained at sizes lower than 75 kDa is ubiquitin conjugated to the degradation products of neurolastin (See Figure S1D).
(D) Detection of neurolastin in the membrane and cytosolic fractions of cells expressing neurolastin-HA. Samples were resolved by SDS-PAGE and immunoblotted with α-HA antibody. HA-atlastin was used as a control. PNS: Post Nuclear supernatant.
(E) Membrane fraction (as generated in D) was subsequently lysed in buffer containing Tx-114 to separate the peripheral (aqueous phase) and integral (detergent phase) membrane proteins. Samples were resolved by SDS-PAGE and immunoblotted with α- HA antibody.
(F) Detection of different truncations of neurolastin in the membrane and cytosolic fractions.
(G) Neurolastin-HA was expressed in HeLa cells and visualized by immunostaining with α-HA antibody (red). Different organelles were stained with specific markers/antibodies: nucleus (DAPI), ER (α-KDEL), mitochondria (α-ATP5A), or Golgi (α-GM130). Scale bar, 10 μm.
(H) GFP-tagged Rabs (green), which localize to specific endocytic compartments (Rab 5-early endosomes; Rab 7 and Rab 9-late endosomes; Rab 11-recycling endosomes), were co-transfected with neurolastin-HA (red) and co-localization was analyzed by immunostaining. Merged images are presented. Scale bar, 10 μm. Inset shows enlarged region.

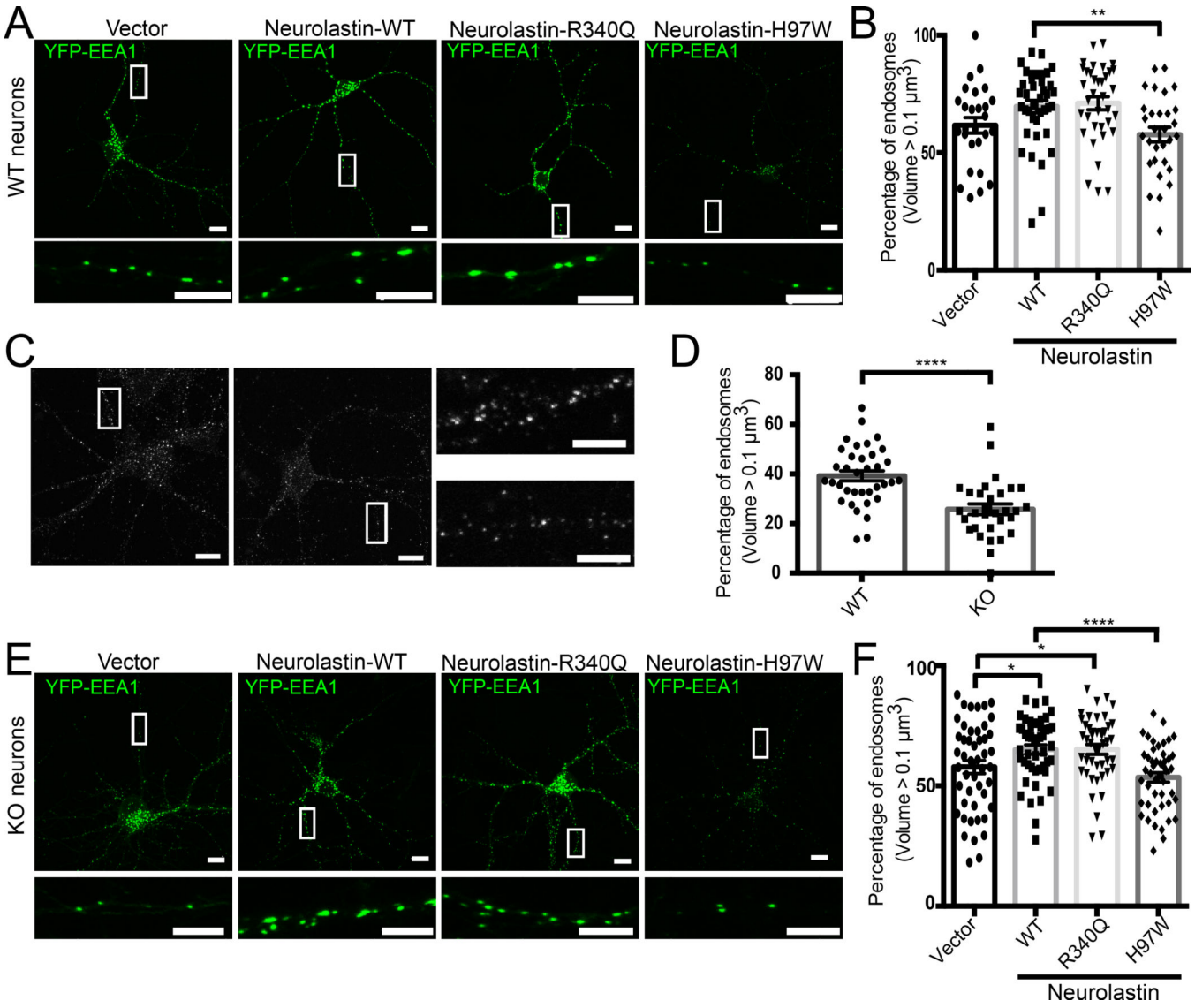

Figure 3. Neurolastin RING domain affects endosome size

(A) Endosomes (labeled with YFP-EEA1) in rat hippocampal neurons transfected with neurolastin-HA (WT or mutants). Scale bar, 10 μm. Enlarged image of the boxed region is shown below each panel. Scale bar, 5 μm.

(B) Percentage of endosomes (volume > 0.1 μm^3) in dendrites per neuron expressing neurolastin (WT, R340Q or H97W). Vector only used as control. Data represent mean ± SEM (N=3; ** $p < 0.005$).

(C) Hippocampal neurons from WT or KO mice stained for endogenous EEA1 at DIV13. Scale bar, 10 μm. Enlarged image of the boxed region is shown below each panel. Scale bar, 5 μm.

(D) Percentage of endosomes (volume > 0.1 μm^3) in dendrites per neuron from WT or KO neurons. Data represent mean ± SEM (N=2; **** $p < 0.0001$).

(E) Rescue experiment in KO mouse neurons. Endosomes (labeled with YFP-EEA1) transfected with neurolastin-HA (WT or mutants). Scale bar, 10 μm. Enlarged image of the boxed region is shown below each panel. Scale bar, 5 μm.

(F) Percentage of endosomes (volume > 0.1 μm^3) in dendrites per neuron expressing neurolastin (WT, R340Q or H97W). Vector only used as a control. Data represent mean ± SEM (N=3; * $p < 0.05$; **** $p < 0.0001$).

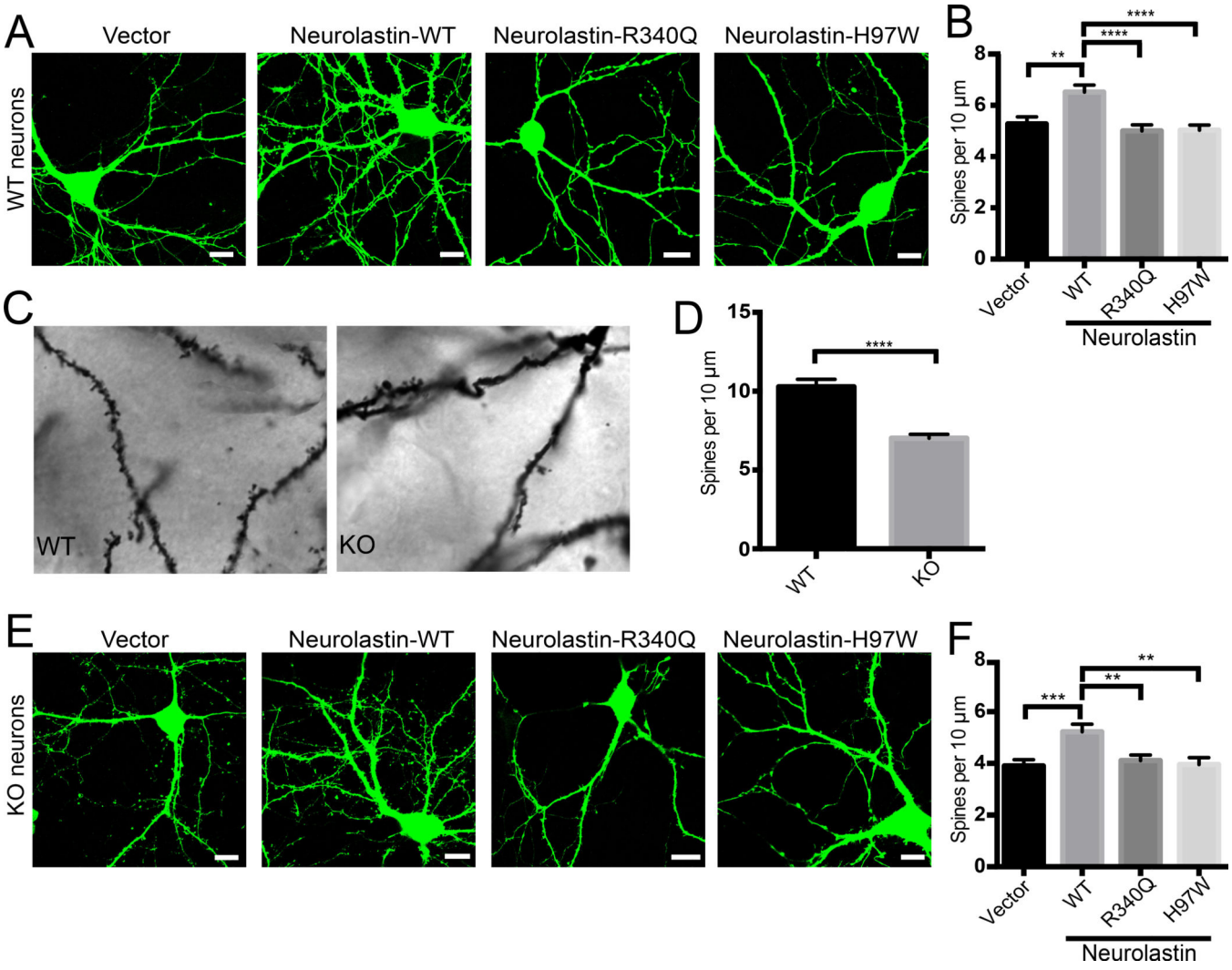

Figure 4.

(A) DIV14 neurons were co-transfected with GFP and neurolastin-HA (WT or mutants). Vector only was used as a control. Cells were fixed at DIV18 and spines were counted (3 dendrites per neuron) using Metamorph analysis software. Scale bar, 10 µm. Graph in **(B)** indicates mean ± SEM of the number of spines per 10 µm length of secondary/tertiary dendrite (N=3 blinded experiments; ** $p < 0.005$; **** $p < 0.0001$).

(C) Golgi stained pyramidal neurons from hippocampus in WT or KO mice (P25–30). Graph in **(D)** represents mean ± SEM of the number of spines per 10 µm length of secondary/tertiary dendrite (N=3; **** $p < 0.0001$).

(E) Rescue experiment in KO mouse neurons. Neurons were transfected at DIV14 and spines visualized at DIV18. Scale bar, 10 µm. Graph in **(F)** shows mean ± SEM of the number of spines per 10 µm length of secondary/tertiary dendrite (N=2 blinded experiments; ** $p < 0.005$; *** $p < 0.001$).

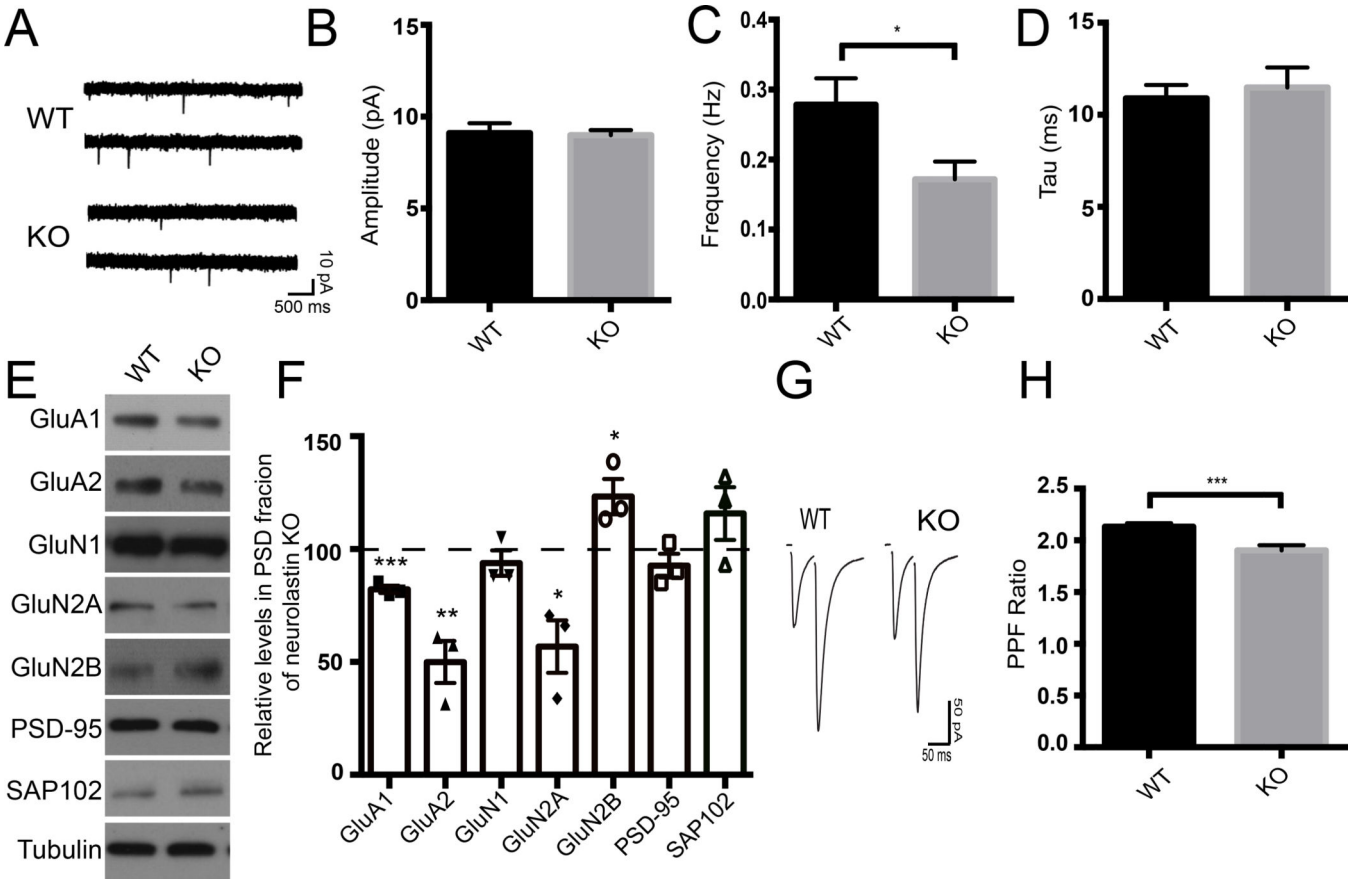

Figure 5. Neurolastin KO mice have impaired synaptic transmission

(A) Representative mEPSC traces recorded in CA1 pyramidal neurons from hippocampal slices of P14–18 mice. Graph indicates mean ± SEM of the amplitude **(B),** frequency **(C)**, and mini decay **(D)** (N=3 blinded experiments; * $p < 0.05$).

(E) Representative Western blot showing levels of different proteins in the synaptic fraction of WT and neurolastin KO mice. Littermates at P16 were analyzed. Graph in **(F)** shows mean ± SEM of relative levels in KO, plotted as percent of WT levels (N=3 independent experiments; * $p < 0.05$; ** $p < 0.01$; *** $p < 0.0005$).

(G) Representative EPSC traces recorded in CA1 pyramidal neurons from hippocampal slices of P14–18 mice. Graph in **(H)** indicates mean ± SEM of the paired pulse ratio with an inter-stimulus interval of 50 ms (N=3 blinded experiments; *** $p < 0.0001$).